Diffusion at the Surface of Topological Insulators

Pierre Adroguer, David Carpentier, Jérôme Cayssol, Edmond Orignac

▶ **To cite this version:**

Pierre Adroguer, David Carpentier, Jérôme Cayssol, Edmond Orignac. Diffusion at the Surface of Topological Insulators. New Journal of Physics, 2012, 14 (10), pp.103027 (1-26). 10.1088/1367-2630/14/10/103027 . hal-00758758

HAL Id: hal-00758758
https://hal.science/hal-00758758v1

Submitted on 13 Mar 2018

HAL is a multi-disciplinary open access archive for the deposit and dissemination of scientific research documents, whether they are published or not. The documents may come from teaching and research institutions in France or abroad, or from public or private research centers.

L'archive ouverte pluridisciplinaire **HAL**, est destinée au dépôt et à la diffusion de documents scientifiques de niveau recherche, publiés ou non, émanant des établissements d'enseignement et de recherche français ou étrangers, des laboratoires publics ou privés.

Distributed under a Creative Commons Attribution - NonCommercial - NoDerivatives 4.0 International License

IOPscience iopscience.iop.org

Home Search Collections Journals About Contact us My IOPscience

Diffusion at the surface of topological insulators

This article has been downloaded from IOPscience. Please scroll down to see the full text article.

2012 New J. Phys. 14 103027

(http://iopscience.iop.org/1367-2630/14/10/103027)

View the table of contents for this issue, or go to the journal homepage for more

Download details:
IP Address: 147.210.24.83
The article was downloaded on 29/11/2012 at 09:40

Please note that terms and conditions apply.

New Journal of Physics
The open-access journal for physics

Diffusion at the surface of topological insulators

Pierre Adroguer[1], David Carpentier[1,5], Jérôme Cayssol[2,3,4] and Edmond Orignac[1]

[1] Laboratoire de Physique, Ecole Normale Supérieure de Lyon and CNRS UMR5672, France
[2] Laboratoire Ondes et Matière d'Aquitaine, CNRS UMR5798, University Bordeaux 1, F-33045 Talence, France
[3] Max-Planck-Institut für Physik komplexer Systeme, 01187 Dresden, Germany
[4] Department of Physics, University of California, Berkeley, CA 94720, USA
E-mail: David.Carpentier@ens-lyon.fr

New Journal of Physics **14** (2012) 103027 (26pp)
Received 1 June 2012
Published 17 October 2012
Online at http://www.njp.org/
doi:10.1088/1367-2630/14/10/103027

Abstract. We consider the dc transport properties of topological insulator surface states in the presence of uncorrelated point-like disorder, both in the classical and quantum regimes. The dc conductivity of those two-dimensional surface states depends strongly on the amplitude of the hexagonal warping of their Fermi surface. A perturbative analysis of the warping is shown to fail to describe the transport in Bi_2Se_3 over a broad range of experimentally available Fermi energies, and in Bi_2Te_3 for the higher Fermi energies. Hence we develop a fully non-perturbative description of these effects. In particular, we find that the dependence of the warping amplitude on the Fermi energy manifests itself in a strong dependence of the diffusion constant on this Fermi energy, leading to several important experimental consequences. Moreover, the combination of a strong warping with an in-plane Zeeman effect leads to an attenuation of conductance fluctuations in contrast to the situation of unwarped Dirac surface states.

[5] Author to whom any correspondence should be addressed.

Content from this work may be used under the terms of the Creative Commons Attribution-NonCommercial-ShareAlike 3.0 licence. Any further distribution of this work must maintain attribution to the author(s) and the title of the work, journal citation and DOI.

© IOP Publishing Ltd and Deutsche Physikalische Gesellschaft

Contents

1. Introduction **2**
2. The model **4**
2.1. Hamiltonian and warping potential 4
3. Classical Drude conductivity: the Boltzmann equation **5**
4. Classical Drude conductivity: the diagrammatic approach **8**
4.1. Averaged Green's function and elastic scattering time 8
4.2. Diagrams for the classical conductivity 8
5. Quantum corrections to the conductivity **11**
5.1. Universality classes 12
5.2. Weak anti-localization 13
5.3. Universal conductance fluctuations 14
5.4. In-plane magnetic field: interplay between Zeeman and warping effects 15
6. Summary of the results and conclusions **16**
Acknowledgments **19**
Appendix A. Non-perturbative density of states **19**
Appendix B. Weak anti-localization correction for Dirac fermions **20**
Appendix C. Universal conductance fluctuations for Dirac fermions **22**
Appendix D. Quantum correction for a warped Fermi surface **23**
References **24**

1. Introduction

Topological insulators (TIs) constitute a new state of matter with an insulating bulk and an odd number of metallic Dirac cones at their surface [1, 2]. It was predicted [3] and confirmed by angle-resolved photoemission spectroscopy (ARPES) [4–6] that the compounds Bi_2Se_3, Bi_2Te_3 and Sb_2Te_3 possess such a single surface state (SS). Owing to this spin locking property, SSs of TIs are unique metallic systems for the study of fundamental magnetotransport properties and for the realization of future spintronics-based devices. Unfortunately, such transport experiments have been facing considerable difficulty so far. Indeed, most TI samples present enough residual bulk conductance to overwhelm the actual surface contribution [7–10]. The Shubnikov–de Haas oscillations reported in Bi_2Se_3 crystals originate exclusively from bulk three-dimensional (3D) bands, indicating a low mobility for the surface Dirac fermions [7–9]. Nevertheless, progress has recently been made by using ultrathin films of Bi_2Se_3 [11–13] or Bi_2Te_3 [14] exfoliated on a high-k dielectric insulator in order to improve the surface/bulk conductance ratio and to allow the gating of the SS. From the gate voltage dependence of the total conductance, it was possible to separate bulk and surface contributions using a classical two-carrier model [11, 12]. Most recently, surface conductance of strained HgTe samples has been reported in truly 3D slabs with thicknesses exceeding 100 nm and in the absence of significant bulk conductance [15]. At low temperatures and for small samples, the quantum correction to transport was recently probed experimentally: the dependence of conductance on weak magnetic fields displays the expected weak anti-localization (WAL), while universal conductance fluctuations (UCF) were observed in some of those experiments [11, 14, 15].

Interestingly, crossover between the symplectic and unitary universality classes upon breaking time-reversal symmetry has been observed in ultrathin samples of Bi_2Te_3 [16].

Theoretically, describing the transport properties of TI SSs amounts to considering the diffusion properties of two-dimensional (2D) Dirac fermions. Indeed, at the lowest order in $k.p$ theory the SS Fermi surface is circular with a spin winding in the plane. At low energy, this 2D conductor shares a number of similarities with graphene, but with the following important differences: the momentum is locked to a real spin as opposed to an A–B sublattice pseudo-spin in graphene, and it has a single Dirac cone as opposed to the fourfold degeneracy of the Dirac cone in graphene. For this simpler Dirac metal, the conductivity and the induced in-plane spin polarization were calculated as functions of the 2D carrier concentration [17]. Far from the Dirac point, surface spin–orbit may generically produce a significant hexagonal warping (HW) of the spin texture. As a result, the Fermi surface exhibits a snowflake or nearly hexagonal Fermi surface depending on the carrier density, and the spin gets tilted out of the plane [18]. Those effects have been confirmed by ARPES and scanning tunneling microscopy experiments performed on Bi_2Te_3 crystals, where HW is particularly strong [19–23], and also in Bi_2Se_3 [24, 25]. Characterizing quantitatively the HW and therefore the amount of out-of-plane spin polarization is a crucial issue in view of potential spintronics applications, and has been the subject of *ab initio* studies [26] and ARPES experiments [22]. This HW is specific to the Dirac metal at the surface of TIs and is different from the trigonal warping encountered at high energies in graphene. Its amplitude is stronger in the metallic regime of high Fermi energy, which is of interest in the present paper: for a full description of transport properties in this regime, it is necessary to include its presence in the model. It has been shown [27, 28] that HW enhances perturbatively the classical Drude conductivity with respect to the unwarped model [17]. However, as we will show in this paper, a description of the effects of this HW requires us to go beyond the previous perturbative descriptions. In this paper, we develop a description of the diffusion of these SSs that is still perturbative in disorder, but non-perturbative in the amplitude of warping.

We investigate theoretically the classical 2D charge diffusion within hexagonally warped SSs using both a standard diagrammatic formalism and a Boltzmann equation approach. In this classical regime, we find that the HW, on the one hand, strongly reduces the density of states and, on the other hand, increases the diffusion coefficient for the Dirac SSs. The combination of both effects is found to correspond to an increase of the classical conductivity as a function of the warping amplitude. Interestingly, as the warping amplitude increases with Fermi energy, that dependence on the warping amplitude manifests itself in the behavior of the conductivity as a function of the Fermi energy. In the second part of this paper, we focus on the quantum correction to the conductivity, relevant in a phase coherent conductor. These quantum corrections are known to depend on the symmetry class of the associated Anderson localization problem. Similar to graphene with only intravalley disorder, the single Dirac cone model is known to correspond to the symplectic/AII class. Within this symplectic class the Dirac model differs from graphene with long-range disorder or electrons with spin–orbit randomness by the presence of a topological term in the associated field theory [29, 30]. This topological term explains the absence of Anderson localization for these TI SSs [31–33]; however, it plays no role in the diffusive metallic regime. In this regime, the universal properties of both weak localization and conductance fluctuations are just the same as for any model in the 2D symplectic/AII class. We will recall these results, and show that the dependence of the diffusion coefficient on warping manifests itself in a dependence of the weak localization correction and conductance

fluctuations away from their universal values. In particular, this diffusion constant parameterizes the universal crossover from the symplectic/AII class to the unitary/A class when a magnetic field is applied perpendicular to the SSs. The shape of the associated crossover functions now depends strongly on the warping amplitude, and thus the Fermi energy. Finally, we identify a property unique to the TI SSs: a reduction of the conductance fluctuations by the application of an in-plane magnetic field.

The paper is organized as follows. We present the model in section 2. The classical Drude conductivity in the presence of HW is derived using a Boltzmann approach (section 3) and a diagrammatic method (section 4). In section 5, the quantum corrections to the average conductivity and the UCF are respectively derived. The results and conclusions relevant to experiments are summarized in section 6.

2. The model

2.1. Hamiltonian and warping potential

We consider the Hamiltonian describing a single species of SSs of a strong TI,

$$H = \hbar v_{\mathrm{F}}\, \vec{\sigma}\cdot\vec{k} + \frac{\lambda}{2}\sigma_z(k_+^3 + k_-^3) + V(\vec{r}), \tag{1}$$

where $\vec{\sigma} = (\sigma_x, \sigma_y)$ is the 2D vector of Pauli matrices describing the physical in-plane spin of the electron and $\vec{k} = (k_x, k_y)$ is its in-plane momentum operator, which satisfies the usual commutation relation with the position operator $[r_\alpha, k_\beta] = \mathrm{i}\delta_{\alpha\beta}$ $(\alpha, \beta = x, y, z)$. Note that in equation (1), we used for the sake of simplicity the dispersion relation $\vec{\sigma}\cdot\vec{k}$ for the Dirac part instead of the usual $\vec{\sigma}\times\vec{k}$ Hamiltonian: switching from one to the other amounts to performing an in-plane $\pi/2$ rotation around z in the spin space and has no consequence on the following discussion as it does not affect the HW potential. Concerning the description of the disorder potential $V(\vec{r})$, we will follow the standard description by considering a Gaussian random potential $V(\vec{r})$, characterized by a zero average value $\langle V(\vec{r})\rangle = 0$ and variance $\langle V(\vec{r})V(\vec{r'})\rangle = \gamma\delta(\vec{r}-\vec{r'})$, where $\langle\cdots\rangle$ represents the average over different disorder realizations.

The HW term $H_{\mathrm{W}} = \frac{\lambda}{2}\sigma_z(k_+^3 + k_-^3)$, with $k_\pm = k_x \pm \mathrm{i}k_y$, breaks the full $U(1)$ rotation symmetry of the Dirac cone down to a trigonal discrete C_3 symmetry [18, 34]. Time-reversal symmetry leads to an additional hexagonal C_6 symmetry of the Fermi surface, hence the name HW (figure 1). The dispersion relation in the absence of disorder with $\vec{k} = (k_x, k_y) = k(\cos\theta, \sin\theta)$:

$$\epsilon^2(\vec{k}) = \hbar^2 v_{\mathrm{F}}^2 k^2 + \lambda^2 k^6 \cos^2(3\theta), \tag{2}$$

is obtained by squaring the Hamiltonian equation (1) with $V(\vec{r}) = 0$ and leads to the snowflake shape of equal energy surfaces at high energies: see figure 1. Defining $E_{\mathrm{F}} = \hbar v_{\mathrm{F}} k_{\mathrm{F}}$ and $k = k_{\mathrm{F}}\tilde{k}(\theta)$, the shape of the Fermi surface at energy E_{F} is defined by the equation

$$1 = \tilde{k}^2(\theta) + 4b^2\tilde{k}^6(\theta)\cos^2(3\theta). \tag{3}$$

Hence the warping of this Fermi surface is naturally characterized by the dimensionless parameter

$$b = \frac{\lambda E_{\mathrm{F}}^2}{2\hbar^3 v_{\mathrm{F}}^3}, \tag{4}$$

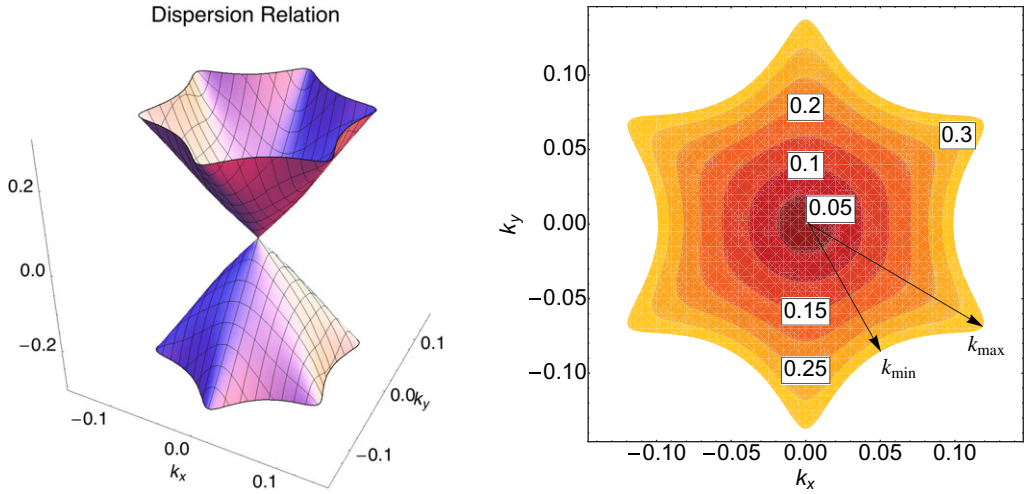

Figure 1. Fermi surface in the presence of HW for various Fermi energies with parameters relevant for Bi_2Te_3: $\lambda = 250\,\text{eV}\,\text{Å}^3$ and $v_F = 2.55\,\text{eV}\,\text{Å}$ and Fermi energies from $E_F = 0.05$ to $0.3\,\text{eV}$, corresponding to a warping parameter b ranging from 0 to $b \simeq 0.7$.

which will play a crucial role in the remainder of this paper. This parameter is related to the geometrical warping deformation factor w introduced in [22], and defined from the maximum and minimum momenta k_{max}, k_{min} of a constant energy contour (see figure 1) as

$$\tilde{w} = \frac{w}{w_{max}} = \frac{k_{max} - k_{min}}{k_{max} + k_{min}} \quad \text{with } w_{max} = \frac{2+\sqrt{3}}{2-\sqrt{3}} \simeq 13.9. \tag{5}$$

With the notations of equation (3), we have $k_{min}/k_{max} = \tilde{k}(\theta = 0)$, leading to the expression

$$b(w) = \frac{\sqrt{\tilde{w}}(1+\tilde{w})^2}{(1-\tilde{w})^3} = \sqrt{w\,w_{max}}\,\frac{(w_{max}+w)^2}{(w_{max}-w)^3}. \tag{6}$$

Two values appear remarkable: $w = 0$, $b = 0$ correspond to a circular Fermi surface; $w = 1$, $b = 2/(3\sqrt{3}) \simeq 0.38$ correspond to a hexagonal Fermi surface; while $w > 1$ indicates a snowflake shape.

Using the experimental values for the Bi_2Se_3 compound $\lambda = 128\,\text{eV}\,\text{Å}^3$, $v_F = 3.55\,\text{eV}\,\text{Å}$ from [24], we obtain relatively small values of warping $0.04 < b < 0.09$ for energies $0.05\,\text{eV} < E < 0.15\,\text{eV}$, and similarly $0.0 < b < 0.04$ with the values $\lambda = 95\,\text{eV}\,\text{Å}^3$, $v_F = 3.0\,\text{eV}\,\text{Å}$ and $0.00\,\text{eV} < E < 0.15\,\text{eV}$ from [25]. On the other hand, the experimental values for the Bi_2Te_3 compound $\lambda = 250\,\text{eV}\,\text{Å}^3$ and $v_F = 2.55\,\text{eV}\,\text{Å}$ [5, 19] lead to a warping factor ranging from $b = 0.13$ for $E = 0.13\,\text{eV}$ to $b = 0.66$ for $E = 0.295\,\text{eV}$. As we will show below, these large values of warping amplitude are indeed beyond the reach of a perturbative approach and require a non-perturbative description of diffusion in the presence of warping.

3. Classical Drude conductivity: the Boltzmann equation

In this section, we derive the expression for the classical Drude conductivity using the Boltzmann equation: this conductivity includes all incoherent contributions and neglects the

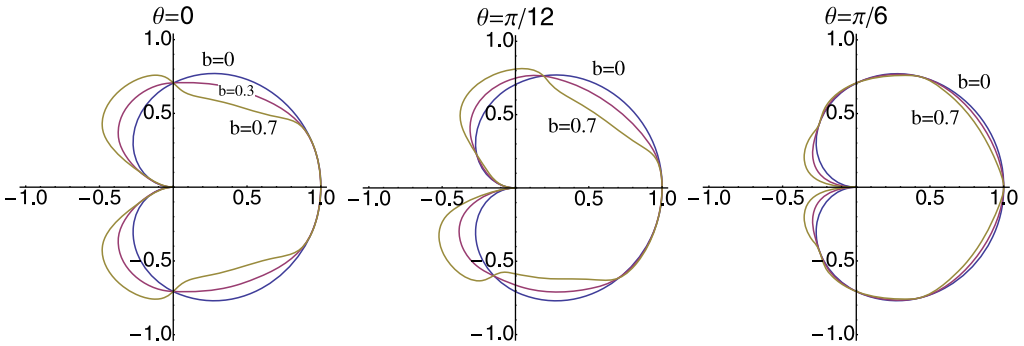

Figure 2. Scattering amplitude $|\langle\vec{k}|V|\vec{k'}\rangle|^2$ plotted as a function of the relative angle $\theta' - \theta$ between the incident state $\vec{k}$ of polar angle θ and the scattered state $\vec{k'}$ of polar angle θ'. Three different incident directions are plotted to demonstrate the dependence on the polar angle of the incident state: $\theta = 0, \pi/12, \pi/6$, while the results are invariant by $\pi/3$ rotation of the incident state. The results are shown for increasing energies warping factor $b = 0$–0.7 corresponding to increasing Fermi energies in a given material.

quantum interference corrections. The momentum relaxation rate in the presence of warping can be obtained from a simple application of Fermi's golden rule:

$$\frac{1}{\tau_e} = \int \frac{d\vec{k'}}{(2\pi)^2} 2\pi |\langle\vec{k'}|\vec{k}\rangle|^2 \gamma \delta(\epsilon(\vec{k'}) - E_F), \tag{7}$$

where $\langle\vec{k'}|\vec{k}\rangle$ is the overlap between the eigenstates labeled by $\vec{k}$ and $\vec{k'}$ at the Fermi surface. The disorder strength is characterized by $\gamma = n_i V^2$ and the dispersion $\epsilon(\vec{k})$ is given by equation (2).

At equilibrium, the occupation numbers are given by the Fermi distribution $n_F(\epsilon(\vec{k}))$. In the presence of a finite external electric field $\vec{E}$, the occupation number function $f(\vec{k})$ has to be determined by solving the Boltzmann equation:

$$-e\vec{E} \cdot \frac{\partial f(\vec{k})}{\partial \vec{k}} = \int \frac{d\vec{k'}}{(2\pi)^2} 2\pi n_i |\langle\vec{k'}|V|\vec{k}\rangle|^2 \delta(\epsilon(\vec{k'}) - \epsilon(\vec{k})) \left[f(\vec{k'}) - f(\vec{k}) \right]. \tag{8}$$

This equation is non-trivial to solve due to both the warped shape of the Fermi surface and the anisotropy of the scattering. Indeed, even if the scalar disorder is isotropic and spin diagonal, the spin-locking property renders the scattering anisotropic (even for a circular unwarped Fermi surface). This anisotropy is further increased by the HW of the Fermi surface. This is apparent when considering the scattering amplitude which appears in equation (8): $f(\theta, \theta' - \theta) = |\langle\vec{k}|V|\vec{k'}\rangle|$ between eigenstates of the disorder-free Hamiltonian $H_0 + H_w$ in equation (1), as a function of the polar angle θ of the incident state $|\vec{k}\rangle$ and polar angle θ' of the outgoing state $|\vec{k'}\rangle$. Due to the presence of HW, this scattering amplitude is highly spin-dependent and anisotropic along the Fermi surface, especially at large Fermi energy where the warping factor b is large. Moreover, this amplitude $f(\theta, \theta' - \theta)$ becomes dependent on the incident state direction θ, and not only on the relative angle, $(\theta' - \theta)$, as opposed to the case of Dirac fermions without warping. These properties are represented in figure 2.

To solve equation (8), we use the linearized ansatz:

$$f(\vec{k}) = n_F(\epsilon(\vec{k})) + \frac{\partial n_F}{\partial \epsilon} \bar{f}(\theta), \tag{9}$$

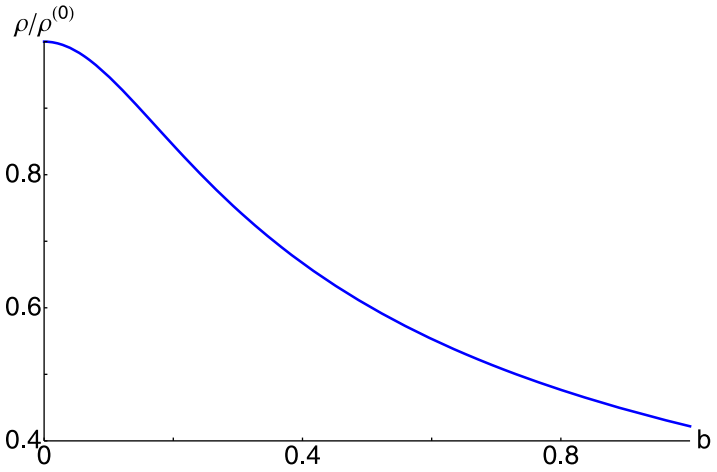

Figure 3. Renormalization of the density of states $\rho(E_F)$ by the warping of the SSs, non-perturbatively in the warping amplitude b. The resulting correction is represented by $\rho(E_F)/\rho^{(0)}$ where $\rho^{(0)} = \rho(\lambda = 0)$ is the density for Dirac fermions without warping.

where the angular function $\bar{f}(\theta)$ is linear in electric field. We find that

$$-e\vec{E}.\frac{\partial\epsilon}{\partial\vec{k}} = 2\pi\gamma \int \frac{d\theta'}{(2\pi)^2} |\langle\vec{k}'|\vec{k}\rangle|^2 k_{F\theta'} \left(\frac{\partial\epsilon}{\partial k}\right)^{-1}_{\theta'} \left[\bar{f}(\theta') - \bar{f}(\theta)\right], \tag{10}$$

where the Fermi wavevector $k_{F\theta'}$ and the derivative $(\partial\epsilon/\partial k)_{\theta'}$ are both evaluated at the point of the Fermi surface labeled by the angle θ'. The solution to this integral equation at fourth order in b is

$$\bar{f}(\theta) = e v_F \tau_e E_x \Big[2\cos\theta + b^2\,(18\cos\theta + 5\cos(5\theta) - \cos(7\theta)) - \frac{b^4}{4}\,(522\cos\theta + 20\cos(5\theta) + 44\cos(7\theta) + 49\cos(11\theta) - 11\cos(13\theta))\Big]. \tag{11}$$

The current is then calculated as

$$j_x = \int \frac{d\vec{k}}{(2\pi)^2} e \frac{\partial\epsilon}{\partial k_x} \bar{f}(\theta)\delta(\epsilon(\vec{k}) - E_F) = \sigma E_x, \tag{12}$$

leading to the conductivity

$$\sigma = \sigma^{(0)}\left(1 + 8b^2 - 58b^4 + o(b^4)\right). \tag{13}$$

The conductivity and density of states (at the Fermi level) in the absence of warping ($b = 0$) are given respectively by $\sigma^{(0)} = e^2\rho^{(0)}v_F^2\tau_e^{(0)}$ and $\rho^{(0)} = \frac{E_F}{2\pi\hbar^2 v_F^2}$. Similarly, one can also derive the perturbative (and non-perturbative) expression for the density of states ρ: this is done in appendix A and the result is represented in figure 3. However, to go beyond the above perturbative expansion for the conductivity, a diagrammatic approach turns out to be more convenient. Hence, we proceed below by developing such an approach, comparing its results with the perturbative expansion of equation (13).

4. Classical Drude conductivity: the diagrammatic approach

In this part, we investigate within the standard diagrammatic framework the diffusive transport of the Dirac SS with an arbitrary large warping deformation (see equation (1)). Within this approach, we still employ the standard description of diffusion perturbative in the disorder (small parameter $1/(k_F l_e)$; but treat the warping potential non-perturbatively (in its amplitude b). We start by calculating the single particle Green function averaged over disorder whose imaginary part yields the density of states. Then we evaluate the classical Drude conductivity from the bubble diagram containing two dressed current operators linked by two disorder averaged Green functions. We discuss the dependence of the classical conductance as a function of the 2D carrier density and the HW coupling strength.

4.1. Averaged Green's function and elastic scattering time

The averaged Green's function is obtained by calculating the self-energy correction and averaging over disorder [35]. The corresponding disorder averaged propagator reads

$$\langle G^{R/A}(\vec{k})\rangle = \frac{(E \pm i\hbar/2\tau_e)\mathbb{1} + \hbar v_F \vec{k} \,.\, \vec{\sigma} + \lambda k^3 \cos(3\theta)\sigma^z}{(E \pm i\hbar/2\tau_e)^2 - \hbar^2 v_F^2 k^2 - \lambda^2 k^6 \cos^2(3\theta)}, \tag{14}$$

where the elastic scattering time for the warped (resp. unwarped) conical Dirac fermion τ_e (resp. $\tau_e^{(0)}$) is defined by

$$\rho\tau_e = \rho^{(0)}\tau_e^{(0)} = \frac{\hbar}{\pi\gamma}. \tag{15}$$

We assume that the phase coherence time $\tau_\phi \gg \tau_e$, in order to be in the regime of coherent transport. By using the parameterization $\tilde{k}(\theta)$ of the Fermi surface shape introduced in equation (3), we obtain the non-perturbative expression for the density of states:

$$\frac{\rho}{\rho^{(0)}} = \alpha(b) = \int_0^{2\pi} \frac{d\theta}{2\pi} \frac{1}{1 + 12\, b^2 \tilde{k}^4(\theta)\cos^2(3\theta)} = \frac{\tau_e^{(0)}}{\tau_e}. \tag{16}$$

We find an increase of the scattering time τ_e by the warping. Hence, in the presence of HW, the SSs of TIs are relaxing the carrier momentum less effectively than without warping. This is a manifestation of the increased anisotropy of the scattering amplitude by the HW correction, illustrated in figure 2. Indeed in the presence of HW, the neighboring states of an incident Dirac fermion have smaller overlaps than states that are $\pm 2\pi/3$ apart, which effectively induces a very anisotropic scattering. Nevertheless, from this result, one cannot yet conclude that the Drude conductance is enhanced as the density of states at the Fermi energy is also renormalized by the warping. Indeed, the Drude conductance is determined by the diffusion constant D and the transport relaxation time rather than the elastic scattering time τ_e governing momentum relaxation. To access this classical conductivity, we follow the standard diagrammatic procedure in the following section.

4.2. Diagrams for the classical conductivity

For a given impurity configuration, the conductivity is given by the Kubo formula

$$\sigma = \sigma_{xx} = \frac{\hbar}{2\pi L^2} \Re \mathrm{Tr}\left[j_x G^R j_x G^A\right], \tag{17}$$

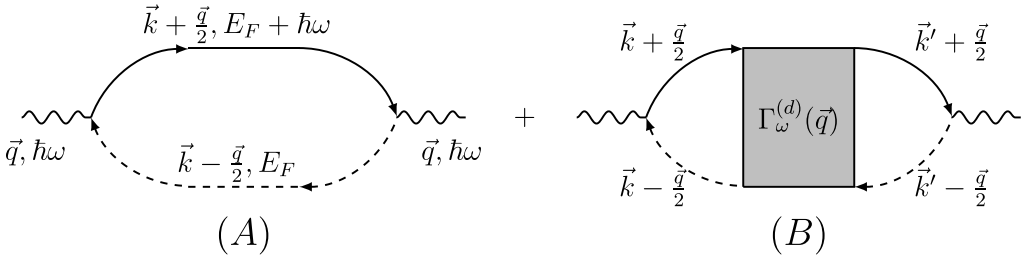

Figure 4. Diagrammatic representation of the two contributions σ_A and σ_B to the classical conductance.

where we have neglected subdominant contributions involving products $G^{\mathrm{R}}G^{\mathrm{R}}$ and $G^{\mathrm{A}}G^{\mathrm{A}}$ [36]. In this expression and below, Tr denotes a trace over the electron's Hilbert space (momentum and spin quantum numbers). The current operator j_α is obtained from the Hamiltonian equation (1) by inserting the vector potential via the minimal coupling substitution $\vec{k} \to \vec{k} - (e/\hbar)\vec{A}$ and using the definition $j_\alpha = \frac{\delta H}{\delta A_\alpha}$:

$$j_x = (-e)\left(v_{\mathrm{F}}\,\sigma_x + \frac{3\lambda}{\hbar}\sigma_z(k_x^2 - k_y^2)\right). \tag{18}$$

Note that this current contains the usual $-ev_{\mathrm{F}}\sigma_x$ term for the linearly dispersing Dirac system, and an additional term quadratic in momentum originating from the HW.

After averaging over all impurity configurations, the classical mean conductivity is obtained from the bubble diagram of figure 4, where the propagating lines represent the retarded and advanced disorder averaged Green functions, equation (14). This classical conductivity is the sum of two terms: σ_A and σ_B.

The contribution of diagram A in figure 4 is defined at $\vec{q} = 0$ and $\omega = 0$ by

$$\sigma_A = \frac{\hbar}{2\pi}\int \frac{\mathrm{d}\vec{k}}{(2\pi)^2}\,\mathrm{tr}[j_x(\vec{k})\langle G^{\mathrm{R}}(\vec{k}, E_{\mathrm{F}})\rangle j_x(\vec{k})\langle G^{\mathrm{A}}(\vec{k}, E_{\mathrm{F}})\rangle], \tag{19}$$

where tr denotes a trace, only over the spin quantum numbers. Performing explicitly the trace and the integration over the momentum $k = |\vec{k}|$, we obtain the following expression:

$$\sigma_A = \frac{\hbar e^2 v_{\mathrm{F}}^2}{2\pi\gamma}\frac{\alpha(b) + 5\beta(b) + \delta(b)}{\alpha(b)}, \tag{20}$$

which is non-perturbative in b. The function $\alpha(b)$ has been defined in equation (16) and we have introduced

$$\alpha(b) = \int_0^{2\pi}\frac{\mathrm{d}\theta}{2\pi}\frac{1}{1 + 12\,b^2\tilde{k}^4(\theta)\cos^2(3\theta)}, \tag{21}$$

$$\beta(b) = \int_0^{2\pi}\frac{\mathrm{d}\theta}{2\pi}\frac{4b^2\cos^2(3\theta)\tilde{k}^6(\theta)}{1 + 12b^2\cos^2(3\theta)\tilde{k}^4(\theta)}, \tag{22}$$

$$\delta(b) = \int_0^{2\pi}\frac{\mathrm{d}\theta}{2\pi}\frac{36b^2(\tilde{k}^4(\theta) - \tilde{k}^6(\theta))}{1 + 12b^2\cos^2(3\theta)\tilde{k}^4(\theta)}, \tag{23}$$

where $k = k_{\mathrm{F}}\tilde{k}(\theta)$ with $\tilde{k}(\theta)$ introduced in equation (3).

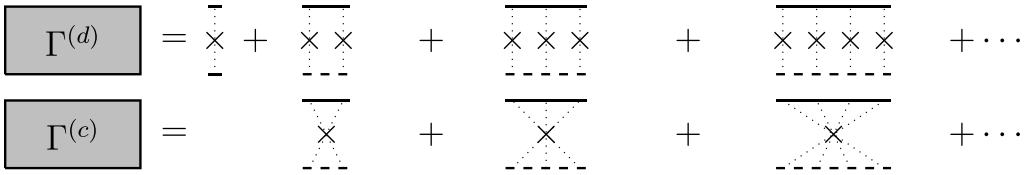

Figure 5. Schematic representation of the Diffuson and Cooperon structure factors. The dotted lines correspond to disorder correlators, while the solid and dashed lines represent retarded and advanced Green's functions.

The contribution of the diagram B in figure 4 accounts for the contribution of the so-called Diffuson [36]. Retaining only the dominant contribution of the integral, we can write it explicitly as

$$\sigma_B(\vec{q},\omega) = \frac{\hbar}{2\pi}\mathrm{tr}\left[J_x \Gamma^{(\mathrm{d})}(\vec{q},\omega) J_x\right], \tag{24}$$

where the vertex operator J is defined by

$$J_x = \int \frac{\mathrm{d}\vec{k}}{(2\pi)^2} \langle G^{\mathrm{A}}(\vec{k},E)\rangle \; j_x(\vec{k}) \; \langle G^{\mathrm{R}}(\vec{k},E)\rangle = J\,\sigma_x. \tag{25}$$

A contraction over the spin indices is assumed, resulting in the proportionality to σ_x.

The Diffuson structure factor $\Gamma^{(\mathrm{d})}$ in equation (24) is defined diagrammatically in figure 5, and satisfies the usual recursive Dyson equation, solved by the expression $\Gamma^{(\mathrm{d})}(\vec{q},\omega) = \gamma\left[\mathbb{1}\otimes\mathbb{1} - \gamma P^{(\mathrm{d})}(\vec{q},\omega)\right]$ where $P^{(\mathrm{d})}$ is the polarizability

$$P^{(\mathrm{d})}(\vec{q},\omega) = \int \frac{\mathrm{d}\vec{k}}{(2\pi)^2} \langle G^{\mathrm{R}}(\vec{k},E)\rangle \otimes \langle G^{\mathrm{A}}(\vec{k}-\vec{q},E-\omega)\rangle, \tag{26}$$

where $\otimes$ denotes a tensor product of the spin Hilbert spaces. The resulting structure factor $\Gamma^{(\mathrm{d})}$ is naturally decomposed into four spin modes. However, as opposed to the case of non-relativistic electrons [36], for finite but small q, the non-diagonal character of the Dirac Green's functions leads to unusual terms in this structure factor such as $(\vec{q}.\vec{\sigma})\otimes(\vec{q}.\vec{\sigma})$, $(\vec{q}.\vec{\sigma})\otimes\mathbb{1}$. We recover the standard singlet and triplet states only in the diffusive $q\to 0$ limit. In this limit, the only gapless mode is the singlet state, characteristic of the symplectic/AII class. While this mode and the associated Cooperon singlet determines the quantum corrections to diffusion, it does not contribute to the classical conductivity of equation (24). The only classical contribution comes from one of the massive triplet states. In full generality, the $q\to 0$ limit of the structure factor $\Gamma^{(\mathrm{d})}$ can be parameterized according to

$$\Gamma^{(\mathrm{d})} = a_1\mathbb{1}\otimes\mathbb{1} + a_2(\sigma^x\otimes\sigma^x + \sigma^y\otimes\sigma^y) + a_3\sigma^z\otimes\sigma^z. \tag{27}$$

Using the parameterization of equation (25) and performing the resulting trace, we obtain

$$\sigma_B = j^2(a_1 - a_3) = \frac{\hbar e^2 v_{\mathrm{F}}^2}{2\pi\gamma}\frac{(\alpha(b)+2\beta(b))^2}{\alpha(b)(\alpha(b)+\beta(b))}. \tag{28}$$

Adding the two contributions of equations (20) and (28) leads to the full expression for the classical conductivity:

$$\sigma_{\mathrm{cl}} = \sigma_A + \sigma_B = e^2\rho D. \tag{29}$$

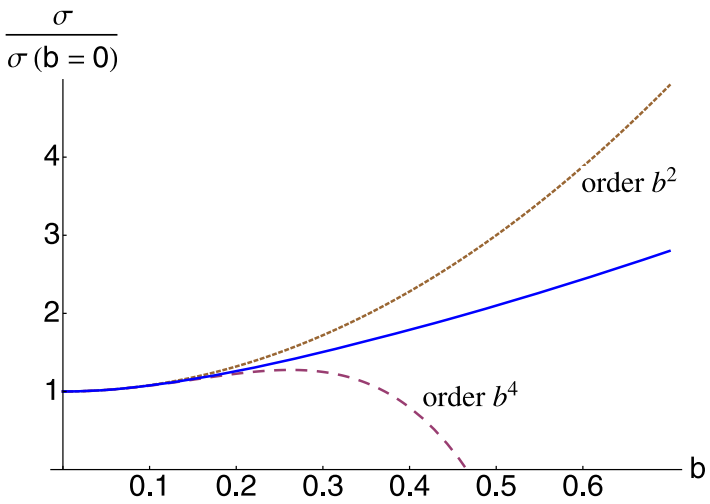

Figure 6. Longitudinal conductivity as a function of the parameter b. The solid line is the exact calculation, the dotted line is the fourth-order expansion in parameter b calculated through the Boltzmann equation and the dashed line is of second order.

The evolution of this classical conductivity as a function of the warping amplitude is represented in figure 6.

Moreover, this expression of the conductivity allows us to define the diffusion constant D from the Einstein relation, whose final expression reads

$$D = \frac{v_F^2 \tau_e}{2} \left(\frac{\alpha(b) + 5\beta(b) + \delta(b)}{\alpha(b)} + \frac{(\alpha(b) + 2\beta(b))^2}{\alpha(b)(\alpha(b) + \beta(b))} \right), \tag{30}$$

which is non-perturbative in the warping parameter b.

In the limit $b \to 0$ of the absence of warping, we recover the known result for Dirac fermions in the presence of scalar disorder with a diffusion constant $D = v_F^2 \tau_e = v_F^2 \tau_{tr}/2$ and a transport time $\tau_{tr} = 2\tau_e$ accounting for the inherent anisotropic scattering of Dirac fermions on scalar disorder. The renormalized diffusion constant is found to increase as a function of b (figure 7). This dramatic increase of D within the range of experimentally relevant warping parameter b signals an effective strong increase of the anisotropy of scattering when HW is present. Note that in the present case, this diffusion coefficient accounts for both the renormalization of the averaged Fermi velocity and the scattering amplitude corresponding to a renormalized transport time. Moreover, the comparison of the expression of equation (30) with its perturbative expansion to order b^4 demonstrates that the experimental values of warping b are beyond the reach of this perturbative expansion (and the similar perturbative studies of [27, 28]): to describe accurately the experimental situation at high doping, the full exact expression equation (30) is required.

5. Quantum corrections to the conductivity

In this section, we focus on the regime of quantum transport corresponding to a phase coherent diffusion of the SSs, which can be reached for small sample size and at low temperatures.

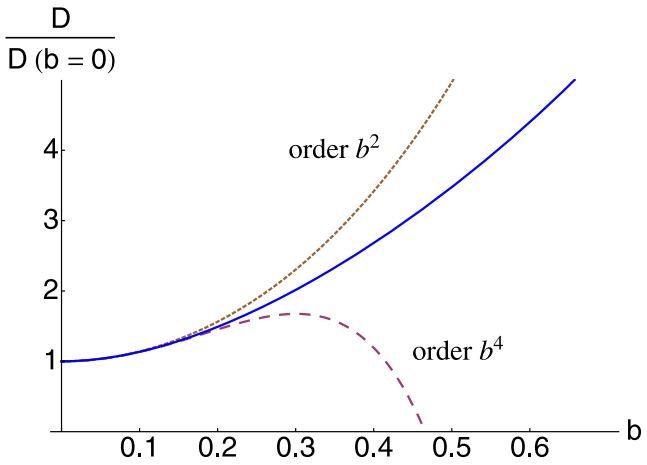

Figure 7. Evolution of the diffusion constant as a function of warping intensity b. The solid line corresponds to the expression non-perturbative in the warping amplitude b, while the dotted and dashed curves correspond to perturbative results to order b^2 and b^4.

This regime corresponds to the situation where the Fermi momentum k_F satisfies the condition $k_F l_e \gg 1$, which naturally corresponds to the situation where the warping of the Fermi surface is strong. We focus on the first two cumulants of the distribution of conductivity and compute diagrammatically the corresponding quantum corrections non-perturbatively in the warping amplitude b, extending the results of [27, 28].

5.1. Universality classes

The study of non-interacting metals perturbed by disorder corresponds to the well-studied problem of Anderson localization of electronic waves. In this framework, the transport properties depend on both dimension and universality classes determined by the symmetries preserved by disorder. These universality classes encode not only the universal properties of the Anderson transition, but also the universal properties of the weak disorder metallic regime of interest experimentally in the present case. The model considered in this paper $H = \hbar v_F \vec{\sigma} \cdot \vec{k} + V(\vec{r})$ is described at large distances by the standard AII/symplectic class: the time-reversal symmetry T is preserved, but due to the momentum-spin locking it squares to $T^2 = -\mathrm{Id}$ [37, 38]. This is also the Anderson universality class describing non-relativistic electrons in the presence of random spin–orbit disorder. However, while both models possess the same universal weak localization properties, they differ in their strong disorder behavior: the topological nature of the single Dirac species in the present model manifests itself in the appearance of a topological term in the field-theoretic description of the $d = 2$ AII class [29, 30]. The presence of this topological $\mathbb{Z}_2$ term modifies the strong disorder/low conductance behavior of the AII class [31–33], but plays no role in the weak disorder regime. Hence the behavior of the first two cumulants in the weak localization regime of the single Dirac model with scalar disorder is exactly that of the standard AII/symplectic class. Moreover, adding the HW term H_w does not break time-reversal symmetry, and thus does not change the universal symmetry class. In contrast, either magnetic disorder or a magnetic field introduced through

a Zeeman or orbital term in the Hamiltonian breaks time-reversal symmetry and induces a crossover from the AII/symplectic to the A/unitary class characterized by the absence of time-reversal symmetry. Such a crossover between the symplectic and unitary ensembles has already been observed by depositing Fe impurities at the surface of ultrathin samples of Bi_2Te_3 [16]. In this experiment, the exchange field of the Fe atoms induces the Zeeman coupling for the SS carriers and destroys the WAL signature. Nevertheless, the extreme thinness of the sample is likely to yield an important hybridization between the bulk and top/bottom SSs while here we consider the response of a single isolated SS.

One of the characterizations of Anderson universality symmetry classes is the number of independent low-energy modes in the diffusive regime. Those modes correspond to the various Cooperon/Diffuson modes which indeed parameterize the target space of the underlying nonlinear sigma field theory. The symplectic class corresponds to two modes, one singlet Diffuson mode and one singlet Cooperon mode [36]. The breaking of time-reversal symmetry by, e.g., an orbital magnetic field will suppress the Cooperons, whose propagator acquires a mass and is no longer diffusive: this induces a crossover from the symplectic class to the unitary class, characterized by a single diffusive mode. This crossover occurs on a length scale determined by the mass acquired by the Cooperon singlet. The suppression of the Cooperon is attributed to destructive interference between time-reversed paths, accounted for by the retarded and advanced Green's functions in the Kubo formula. Such a crossover will be discussed in section 5.4.

5.2. Weak anti-localization

When winding around the Fermi surface, the spinorial electron wave function acquires a π Berry phase which is responsible for the WAL phenomenon. In graphene, the presence of intervalley scattering leads to a crossover from weak anti-localization to weak localization when the ratio of intervalley over intravalley scattering rates is increased [35, 39]. In contrast, TIs with a single Dirac cone provide ideal systems to measure WAL once the issue of the spurious bulk conductance is solved. Actually, some experiments have already reported a strong WAL signal in thin films and in 3D HgTe slabs [15].

The quantum correction to the conductivity in class AII corresponds to a WAL correction: its determination within diagrammatic theory for Dirac fermions is recalled in appendix B. In the limit of a phase coherent sample of size $L_\phi \ll L$, where L_ϕ is the phase coherent length, it reads

$$\langle \delta\sigma \rangle = \left(\frac{e^2}{\pi\hbar}\right) \int_{\tilde{Q}} \frac{1}{Q^2} = \frac{e^2}{\pi h} \ln(L_\phi/\ell_e), \tag{31}$$

where ℓ_e is the elastic mean free path. This result is independent of the particular model within class AII. However, it depends on the amplitude b of warping at high Fermi energy through the diffusion coefficient entering the phase coherence length $L_\phi = \sqrt{D(b)\tau_\phi}$, where τ_ϕ is the phase coherence time.

When a transverse magnetic field is applied, the standard derivation to account for the magnetic orbital effect of this result still holds [36]: it amounts to deriving the Cooperon contribution from the probability of return to the origin of a diffusive path in the presence of the magnetic field. The corresponding correction to conductivity is thus given by [36]

$$\langle \delta\sigma(B) \rangle = \frac{e^2}{4\pi^2\hbar} \left[\Psi\left(\frac{1}{2} + \frac{B_e}{B}\right) - \Psi\left(\frac{1}{2} + \frac{B_\phi}{B}\right) \right], \tag{32}$$

where the characteristic fields $B_e = \hbar/(4eD(b)\tau_e)$ and $B_\phi = \hbar/(4eD(b)\tau_\phi)$ have been introduced, and where Ψ is the Digamma function. The diffusion constant $D(b)$, non-perturbative in b, is given by equation (30). This corresponds to the result obtained for graphene when intervalley scattering can be neglected [35]. In our case, this expression implies that, in a given sample, the shape of the WAL correction as a function of B will evolve as the Fermi energy is varied within the TI gap and the warping amplitude b is varied. This effect will be discussed further in section 6.

5.3. *Universal conductance fluctuations*

As explained above, in the absence of magnetic field the UCF result for the symplectic class results still holds and one finds, similarly to graphene [40],

$$\langle \delta\sigma^2 \rangle = 12 \left(\frac{e^2}{h}\right)^2 \frac{1}{V} \int_{\vec{q}} \frac{1}{q^4}. \tag{33}$$

The derivation of this result for Dirac fermions is recalled in appendix C. Defining the phase coherent $L_\phi = \sqrt{D(b)\tau_\phi(T)}$ and thermal length scales $L_T = \sqrt{\hbar D(b)/T}$, we can focus on different regimes: for $L \ll L_\phi, L_T$, a proper regularization of the integral in (33) leads to the universal value

$$\langle \delta\sigma^2 \rangle = \frac{12}{\pi^4} \left(\frac{e^2}{h}\right)^2 \sum_{n_x=1}^{\infty} \sum_{n_y=0}^{\infty} \frac{1}{(n_x^2 + n_y^2)^2}, \tag{34}$$

where the sum [41]

$$\sum_{n_x=1}^{\infty} \sum_{n_y=0}^{\infty} \frac{1}{(n_x^2 + n_y^2)^2} = \zeta(2)\beta(2), \tag{35}$$

with Catalan's constant [42] $\beta(2) = 0.915\,96\ldots$ and $\zeta(2) = \pi^2/6$, so that

$$\langle \delta\sigma^2 \rangle = \simeq 0.185\,613 \left(\frac{e^2}{h}\right)^2. \tag{36}$$

This result is independent of the diffusion coefficient $D(b)$ and thus independent of the warping amplitude. On the other hand, in the other limits [36]:

$$\langle \delta\sigma^2 \rangle \simeq \frac{3}{\pi} \left(\frac{e^2}{h}\right)^2 \left(\frac{L_\phi}{L}\right)^2 \qquad \text{for } L_\phi \ll L, L_T, \tag{37}$$

$$\simeq \left(\frac{L_T}{L}\right)^2 \left(\frac{e^2}{h}\right)^2 \ln\left(\frac{L}{L_T}\right) \qquad \text{for } L_T \ll L \ll L_\phi, \tag{38}$$

$$\simeq \left(\frac{L_T}{L}\right)^2 \left(\frac{e^2}{h}\right)^2 \ln\left(\frac{L_\phi}{L_T}\right) \qquad \text{for } L_T \ll L_\phi \ll L. \tag{39}$$

Hence a strong dependence of these UCF on the Fermi energy through the warping amplitude b is found in all these cases. The introduction of a transverse magnetic field induces a crossover

from the symplectic class to the unitary class, where the amplitude of the fluctuations is reduced by a factor of 2. This crossover is described as [36]

$$\langle \delta\sigma(B)^2 \rangle = \frac{1}{2}\langle \delta\sigma^2 \rangle \left[1 + \frac{B_\phi}{B} \Psi' \left(\frac{1}{2} + \frac{B_\phi}{B} \right) \right], \tag{40}$$

where Ψ is the Digamma function and $B_\phi(b) = \hbar/4eD(b)\tau_\phi$. The dependence of b on the diffusion constant will affect the value of B_ϕ: this characteristic field for the suppression of the WAL correction and this reduction by a factor of 2 of the conductance fluctuations will decrease when the Fermi level is raised away from the Dirac point.

5.4. In-plane magnetic field: interplay between Zeeman and warping effects

We now consider the effect of an in-plane Zeeman field on the transport properties of these Dirac fermions. This can be accounted for by adding to Hamiltonian (1) a term

$$H_Z = g\mu_B \left(\sigma_x B_x + \sigma_y B_y \right). \tag{41}$$

Without warping, such a Zeeman field acts exactly like a constant vector potential and can be gauged away. This amounts to shifting the momenta uniformly by $-g\mu_B \vec{B}/(\hbar v_F)$. Hence, without warping, an in-plane Zeeman field does not modify the scattering properties of an (infinite) disordered sample. However, the presence of the HW term in (1) breaks this invariance: the shape of the Fermi surface is now modified by the Zeeman field. As a consequence, the scattering amplitudes $f(\theta, \theta' - \theta)$ acquire also a $\vec{B}$ dependence. We can naturally expect that this Zeeman field which modifies the scattering amplitudes redistributes the scattering matrix of the samples, and leads to conductance fluctuations induced by an in-plane magnetic field.

To describe quantitatively the effect of this Zeeman field, we extend the above diagrammatic analysis perturbatively in $\tilde{B} = g\mu_B B/E_F$. This Zeeman field, which breaks time-reversal symmetry, induces a crossover from the symplectic to the unitary class. This crossover can be accounted for by the evolution of the Cooperon structure factor: its singular part no longer corresponds to a diffusive singlet component but to the diffusion of a massive singlet:

$$\Gamma^C(\vec{Q}) = \frac{\gamma}{Dq^2\tau_e + m(b, \tilde{B})} |S\rangle\langle S|. \tag{42}$$

The mass $m(b, \tilde{B})$, which encodes the effects of the Zeeman field, is calculated perturbatively to the second order in $\tilde{B}$: $m(b, \tilde{B}) = m(b)\tilde{B}^2$. The non-perturbative result is represented in figure 8. We recover the expected result $m(0, \tilde{B}) = m(b, 0) = 0$ corresponding to the single singlet diffusive Cooperon mode of the symplectic class.

This mass is associated with a length parameterizing the crossover from the symplectic to the unitary class, defined by $L_B = \sqrt{D\tau_e/m(b, B)}$. Beyond this length scale, we recover a standard unitary weak localization, and conductance fluctuations are reduced by a factor of 2:

$$\langle \delta\sigma(\vec{B}) \rangle = \left(\frac{e^2}{\pi\hbar} \right) \int_{\vec{Q}} \frac{1}{Q^2 + L_B^{-2} + L_\phi^{-2}} = f(\tilde{L}/\ell_e, L/\tilde{L}), \tag{43}$$

$$\begin{aligned} \langle \delta\sigma^2(\vec{B}) \rangle &= 6 \left(\frac{e^2}{h} \right)^2 \frac{1}{V} \left[\int_{\vec{q}} \frac{1}{(q^2 + L_\phi^{-2})^2} + \int_{\vec{q}} \frac{1}{(q^2 + L_B^{-2} + L_\phi^{-2})^2} \right] \\ &= \frac{1}{2}\langle \delta\sigma^2(\vec{B} = \vec{0}) \rangle + f_2(L/\tilde{L}), \end{aligned} \tag{44}$$

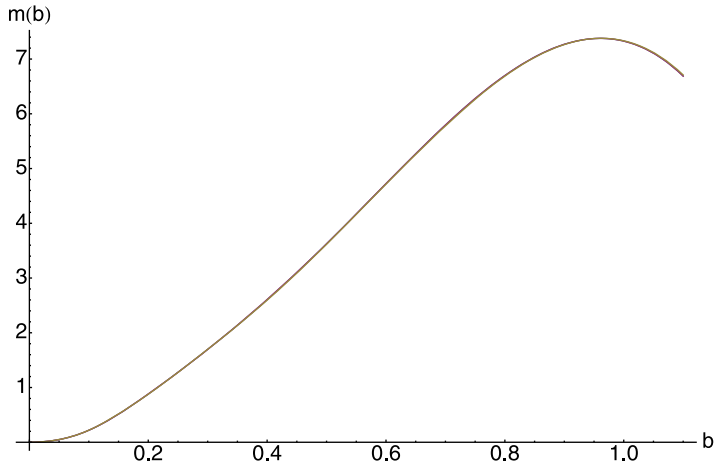

Figure 8. Evolution of the mass term $m(b)$ in the diffusion equation of the Cooperon, in the presence of the HW and in-plane Zeeman magnetic field, as a function of the warping parameter b.

where L is the longitudinal size of the TI surface, L_ϕ is the phase coherence length and $\tilde{L}$ is defined as $\tilde{L}^{-2} = L_B^{-2} + L_\phi^{-2}$. The functions f and f_2 depend on the geometry of the sample. In the case of an infinite 2D sample, one recovers only a logarithmic dependence on $\tilde{L}/\ell_e$ for f. For a finite size sample, one has to replace the integral by a sum over the compatible wavevectors [36].

As expected, we find that the UCF extrapolate between the value for the symplectic and the unitary class, over the length scale $L_B(b, B)$. An estimation of the evaluation of this length as a function of the magnetic field or the warping term is given by

$$\frac{L_B}{\ell_e} = \frac{\sqrt{D(b)/D(b=0)m(b)}}{\tilde{B}} = \frac{c(b)}{\tilde{B}}, \tag{45}$$

where the evolution $c(b)$ with the warping amplitude is shown in figure 9 For experimentally realistic values, $b \simeq 0.7$, $c(0.7) \simeq 1$, $E_F \simeq 0.3\,\text{eV}$ and $g\mu_B \simeq 5 \times 10^{-4}\,\text{eV T}^{-1}$. This gives for a magnetic field around 1 T a characteristic length to observe the crossover $L_B \simeq 1000\,\ell_e$, which is within experimental reach.

The in-plane magnetic field will also induce a competing dephasing effect when threading the finite width penetration region of the SSs. This phenomenon was considered in [27]: with l_{tr} the transport time and λ the penetration length of the SSs the characteristic magnetic field for this effect reads $B_c = \hbar/(e\sqrt{L_\phi l_{tr}}\lambda)$, likely to be shorter than the Zeeman characteristic field in common materials.

6. Summary of the results and conclusions

In this section, we summarize the main results of our approach focusing on the experimentally relevant aspects. In particular, we emphasize the effect of strong variation of the warping amplitude b as the Fermi energy is varied in a given material. The universal properties of transport in the quantum regime are not affected by the presence of this warping. However,

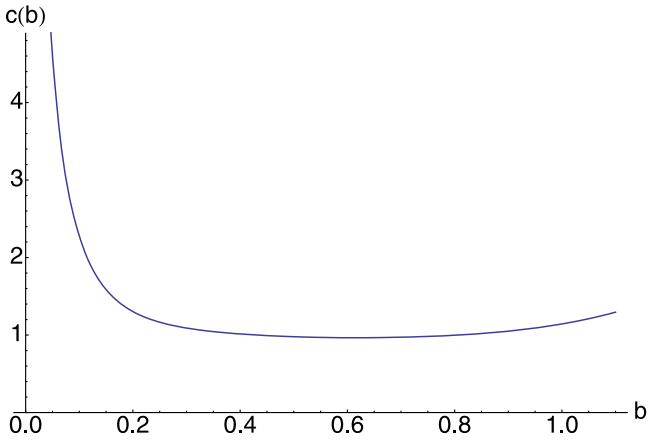

Figure 9. Dependence of b on the characteristic length to observe the crossover from the symplectic to the unitary class, for an in-plane Zeeman magnetic field.

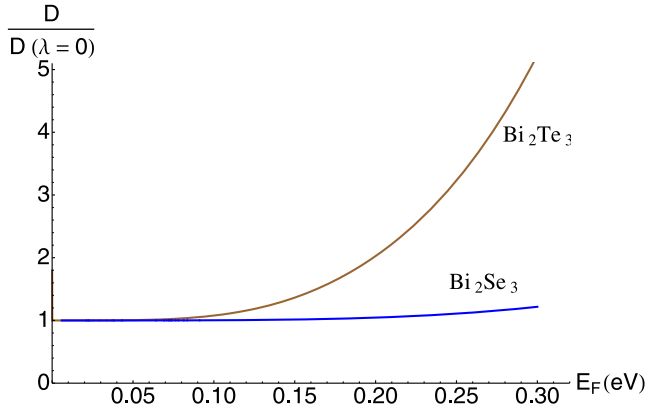

Figure 10. Dependence of the diffusion constant on the Fermi energy for the values of λ, v_F corresponding to the Bi_2Se_3 and Bi_2Te_3 compounds. The results depend on the amplitude of disorder parameterized by the mean free path l_e. Here, they are normalized with respect to the diffusion constant in the absence of warping $D(\lambda = 0)$, which is independent of the Fermi energy and incorporates the dependence on l_e.

both the departure from these universal properties as well as the classical regime are entirely characterized by the diffusion constant $D(b)$, which itself depends on the warping amplitude.

The transport properties in the incoherent classical regime are characterized by both the density of states $\rho(E_F)$ and the diffusion constant D. The dependence on the Fermi energy of both quantities is strongly affected by the presence of the warping of the Fermi surface, whose amplitude b itself depends on E_F. This is shown in figures 10 and 11 for two sets of parameters corresponding to the Bi_2Se_3 and Bi_2Te_3 compounds. As a consequence of these results, the conductivity σ acquires a strong Fermi energy dependence shown in figure 11, which can be directly probed experimentally.

Similarly, the quantum corrections to transport depend strongly on the Fermi energy through the dependence of the diffusion coefficient D on the warping amplitude. Indeed,

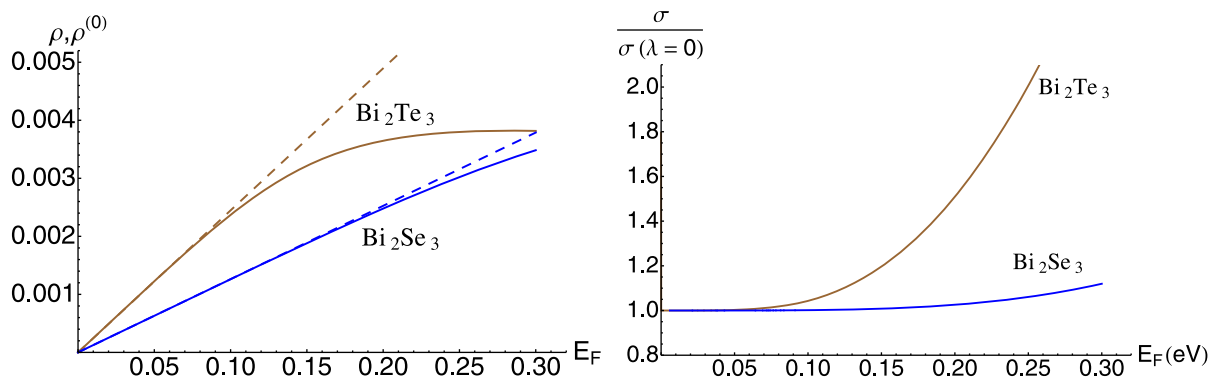

Figure 11. Dependence of the density of states (left) and classical conductivity (right) on the Fermi energy for values of $\lambda = 128\,\text{eV}\,\text{Å}^3$, $v_\text{F} = 3.55\,\text{eV}\,\text{Å}$ for Bi_2Se_3 and $\lambda = 250\,\text{eV}\,\text{Å}^3$ and $v_\text{F} = 2.55\,\text{eV}\,\text{Å}$ corresponding to the Bi_2Te_3 compounds. In the left figure, the dashed lines correspond to the standard linear density of states for Dirac fermions without warping $\lambda = 0$. In the right figure, the results are represented as a ratio with the conductivity in the absence of warping $\sigma(\lambda = 0)$, which is independent of the energy and incorporates the dependence on the disorder strength.

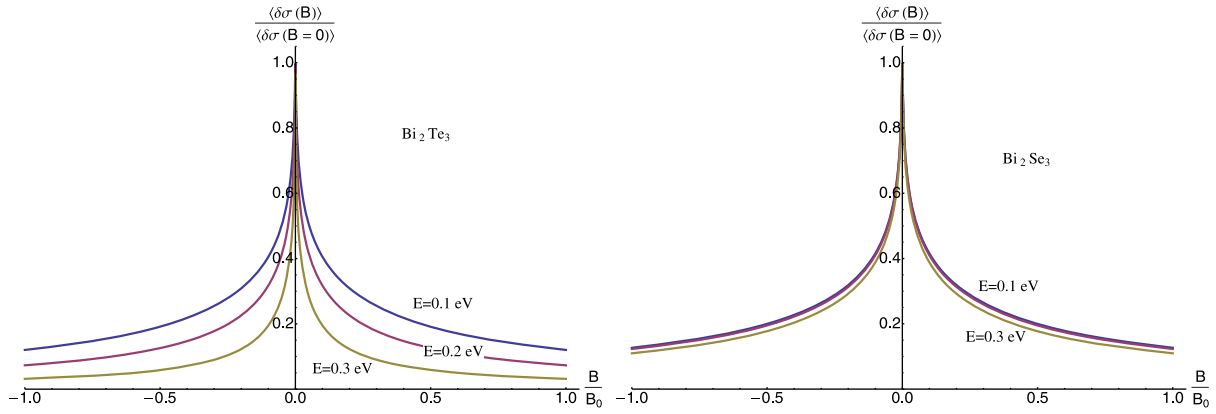

Figure 12. Dependence of the weak localization correction $\langle\delta\sigma(B)\rangle/\langle\delta\sigma(B = 0)\rangle$ on the Fermi energy for the values of λ, v_F corresponding to the Bi_2Te_3 (left) and Bi_2Se_3 (right) compounds. We have chosen to scale the magnetic field as B/B_0 where $B_0 l_\text{e}^2 = \phi_0 = h/e$ to avoid any energy (or warping) dependence of this rescaling field. The results show a clear dependence of energy of the magnetic field characteristic of weak localization decay.

the shape of the typical measurement of the weak (anti-)localization correction through the dependence of the conductivity on a magnetic field perpendicular to the surface depends solely on the diffusion constant. This diffusion constant depending on the Fermi energy, the associated anti-localization curve itself depends on this Fermi energy as shown in figure 12.

While the amplitude of conductance fluctuations is universal in the limit of an entirely coherent conductor, their amplitude in a realistic situation where $L_\phi \simeq L$ will be parameterized by a universal function of the diffusion coefficient. We have shown, moreover that these

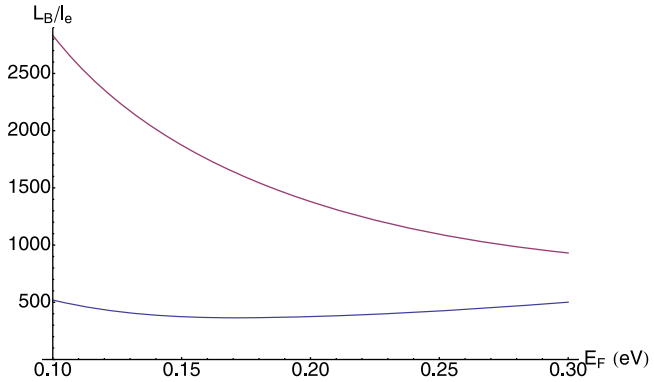

Figure 13. Dependence of the magnetic dephasing length L_B on the Fermi energy for parameters corresponding to Bi_2Te_3 (red) and Bi_2Se_3 compounds.

fluctuations depend in a remarkable way on an in-plane Zeeman magnetic field. The amplitude of this effect depends on the ratio between the associated magnetic dephasing length L_B and the mean free path ℓ_e. The dependence of this ratio on the Fermi energy is shown in figure 13 for the two same sets of values used above.

In conclusion, we have shown that it is essential to take into account the hexagonal deformation of the Dirac cone occurring at the surface of TIs such as Bi_2Se_3 and Bi_2Te_3 to accurately describe both their classical and quantum transport properties. In particular, we provide a formula describing the evolution of diffusion constant D for arbitrary strength of the warping. Since this warping amplitude increases with the Fermi energy of the SSs, we predict a dependence on doping of transport properties different from those predicted for a perfect Dirac cone.

Acknowledgments

This work was supported by the ANR under project no. 2010-BLANC-041902 (ISOTOP). JC acknowledges support from EU/FP7 under the contract TEMSSOC.

Appendix A. Non-perturbative density of states

In the presence of warping, the density of states at the Fermi level $\rho(\epsilon_F)$ is modified. One has

$$\rho(\epsilon) = \int_0^{+\infty} \frac{k\,\mathrm{d}k}{2\pi} \int_0^{2\pi} \frac{\mathrm{d}\theta}{2\pi} \delta\left[\epsilon - \sqrt{(\hbar v k)^2 + \lambda^2 k^6 \cos^2(3\theta)}\right]. \tag{A.1}$$

Performing the angular integration first, the density of states is obtained as the integral

$$\rho(\epsilon) = \frac{\epsilon}{2(\pi\hbar v)^2} \int_{y_-}^{1} \frac{\mathrm{d}y}{\sqrt{(1-y)(4b^2y^3+y-1)}}, \tag{A.2}$$

where y_- is the unique real solution of the equation $4b^2y^3 + y - 1 = 0$. By the usual formula for solving equations of the third degree, we have

$$y_- = \frac{1}{2\sqrt{3}b}\left[\sqrt[3]{3\sqrt{3}b + \sqrt{1+27b^2}} - \sqrt[3]{\sqrt{1+27b^2} - 3\sqrt{3}b}\right]. \tag{A.3}$$

It is convenient to introduce the parameterization $\sinh\varphi = 3\sqrt{3}b$, giving $y_- = 3\sinh(\varphi/3)/\sinh\varphi$. With the change of variables $y_- = 1 - 1/t$, the integral in (A.2) can be rewritten as

$$\rho(\epsilon) = \frac{\epsilon}{2\sqrt{2}b(\pi\hbar v)^2}\int_{t_-}^{+\infty}\frac{\mathrm{d}t}{\sqrt{(t-1)^3 - t^2/(2b^2)}}. \tag{A.4}$$

Using equations (17.4.70)–(17.4.72) from [42], the integral in equation (A.4) can be expressed in terms of a complete elliptic integral of the first kind, giving the density of states:

$$\rho(\epsilon) = \frac{\epsilon}{2(\pi\hbar v)^2}\frac{2K\left[\frac{1}{2} - \frac{1}{4}\left(3 - \frac{1}{\left(1+\frac{4}{3}\sinh^2(\varphi/3)\right)^2}\right)\sqrt{\frac{1+\frac{4}{3}\sinh^2(\varphi/3)}{1+4\sinh^2(\varphi/3)}}\right]}{\left(1+\frac{4}{3}\sinh^2(\varphi/3)\right)^{3/4}\left(1+4\sinh^2(\varphi/3)\right)^{1/4}}. \tag{A.5}$$

In the limit of $\lambda \to 0, \varphi \to 0$, (A.5) reduces to the density of states in the absence of warping. For large λ, we have $b \sim 2\mathrm{e}^{\varphi}3\sqrt{3}$, and the density of states behaves as: $\rho(\epsilon) \sim 3^{-1/4}\pi^{-2}K(1/2 - \sqrt{3}/4)(\epsilon\lambda^2)^{-1/3}$. Since the density of states goes to zero for large and small energy, it has a maximum at a finite value of ϵ. By simple scaling, the maximum is obtained for an energy $\epsilon^* = C_1\sqrt{(\hbar v_\mathrm{F})^3/\lambda}$ and $\rho(\epsilon^*) = C_2(\hbar v_\mathrm{F}\lambda)^{-1/2}$.

Appendix B. Weak anti-localization correction for Dirac fermions

In this appendix, we derive the quantum correction to conductivity for 2D Dirac fermions in the absence of warping ($b = 0$). In this case of linearly dispersing Dirac fermions, the current operator $j_x = -ev_\mathrm{F}\sigma^x$ is no longer a function of $\vec{k}$. The renormalization of this current operator by vertex corrections can be written as

$$\Sigma^x = j_x + j_x P^\mathrm{D}\Gamma^\mathrm{D} = 2j_x, \tag{B.1}$$

where Σ^x stands for the renormalized operator. The quantum corrections to conductivity are associated with contributions between interferences of loops of diffusive paths. This interference between a loop and its time-reversed contribution is described as the propagation of the so-called *Cooperon*. Its propagator is defined through the Dyson equation $\Gamma^\mathrm{C}(\vec{Q},\omega) = \gamma[\mathbb{1}\otimes\mathbb{1} - \gamma P^\mathrm{C}(\vec{Q},\omega)]$, where P^C is

$$P^{(\mathrm{C})}(\vec{Q},\omega) = \int\frac{\mathrm{d}\vec{k}}{(2\pi)^2}\langle G^\mathrm{R}(\vec{k},E)\rangle\,\langle G^\mathrm{A}(\vec{Q}-\vec{k},E-\omega)\rangle. \tag{B.2}$$

By a time-reversal operation on the advanced component, we can relate the Cooperon to the previously identified Diffuson propagator. Only the diffusive modes of the Cooperon contribute to the dominant quantum correction, leading to a structure factor for the Cooperon:

$$\Gamma^\mathrm{C}(\vec{Q}) = \frac{\gamma}{\tau_\mathrm{e}}\frac{1}{DQ^2}|S\rangle\langle S| \tag{B.3}$$

$$= \frac{\gamma}{\tau_\mathrm{e}}\frac{1}{DQ^2}\frac{1}{4}\left[\mathbb{1}\otimes\mathbb{1} - \sigma^x\otimes\sigma^x - \sigma^y\otimes\sigma^y - \sigma^z\otimes\sigma^z\right], \tag{B.4}$$

where D is the diffusion constant, $D = v_\mathrm{F}^2\tau_\mathrm{e}$ in the absence of warping.

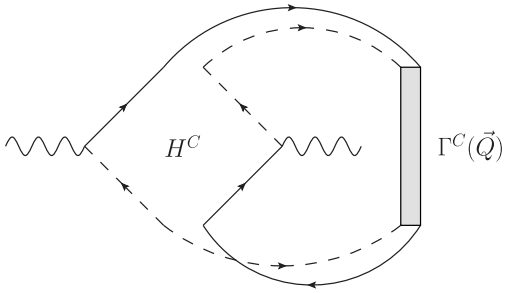

Figure B.1. Diagrammatic representation of the quantum correction to conductivity.

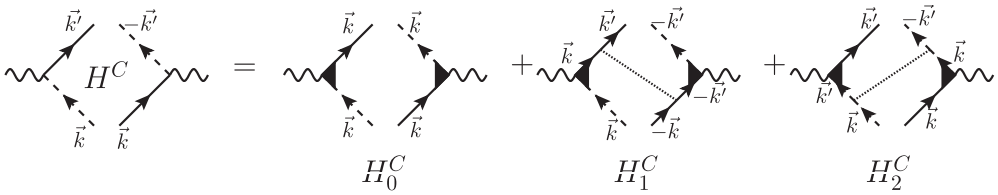

Figure B.2. Diagrammatic representation of the dressing of the Hikami box.

The WAL correction is obtained by the contraction of a Cooperon propagator and a Hikami box, as represented diagrammatically in figure B.1. This Hikami box is the sum of three different contributions represented in figure B.2. We express the first of these contributions as

$$\langle \delta\sigma_0 \rangle = \frac{\hbar}{2\pi} \mathrm{Tr}\left[G^{\mathrm{A}}(\vec{k}) \Sigma^x G^{\mathrm{R}}(\vec{k}) \Gamma^{\mathrm{C}}(\vec{Q}) G^{\mathrm{R}}(\vec{Q}-\vec{k}) \Sigma^x G^{\mathrm{A}}(\vec{Q}-\vec{k}) \right], \tag{B.5}$$

where we used the notations introduced in the paper: Tr for the trace over all the quantum numbers (spin and momenta), tr for the trace over the spin indices and $\int_{\vec{k}}$ for the trace over the momentum $\vec{k}$. Special attention has to be devoted to the order of the spin indices in these expressions. In the expression (B.5), the $\vec{Q}$ integral is dominated by the small $\vec{Q}$ contribution originating from the diffusive modes of the Cooperon. This justifies *a posteriori* the projection on the single diffusive mode in (B.3). Focusing on the most dominant part of this expression, we can set $Q \to 0$ except in the Cooperon propagator, the Green's functions being regular in $\vec{k}$. Similarly, we can pull the renormalized vertices out of the integral and focus on the Hikami box:

$$\begin{aligned} H_0^{\mathrm{C}} &= 4 \int_{\vec{k}} \left[G^{\mathrm{A}}(\vec{k}) \sigma^x G^{\mathrm{R}}(\vec{k}) \right] \otimes \left[G^{\mathrm{R}}(-\vec{k}) \sigma^x G^{\mathrm{A}}(-\vec{k}) \right] \\ &= \rho(E_{\mathrm{F}}) \left(\frac{2\tau_{\mathrm{e}}}{\hbar} \right)^3 \frac{\pi}{16} \left[3\sigma^x \otimes \sigma^x + \sigma^y \otimes \sigma^y - 4\, \mathbb{1} \otimes \mathbb{1} \right]. \end{aligned} \tag{B.6}$$

Similarly, the two remaining diagrams contributing to the Hikami box in figure B.2 are expressed as

$$\begin{aligned} H_1^{\mathrm{C}} &= 4\gamma \int_{\vec{k}} \int_{\vec{q}_1} \left[G^{\mathrm{A}}(\vec{k}) \sigma^x G^{\mathrm{R}}(\vec{k}) G^{\mathrm{R}}(-\vec{q}_1) \right] \otimes \left[G^{\mathrm{R}}(-\vec{k}) G^{\mathrm{R}}(\vec{q}_1) \sigma^x G^{\mathrm{A}}(\vec{q}_1) \right] \\ &= \frac{\pi}{16} \rho(E_{\mathrm{F}}) \left(\frac{2\tau_{\mathrm{e}}}{\hbar} \right)^3 \left[\mathbb{1} \otimes \mathbb{1} - \sigma^x \otimes \sigma^x \right], \end{aligned} \tag{B.7}$$

and

$$H_2^{\mathrm{C}} = 4\gamma \int_{\vec{k}} \int_{\vec{q}_1} \left[G^{\mathrm{A}}(-\vec{q}_1) G^{\mathrm{A}}(\vec{k}) \sigma^x G^{\mathrm{R}}(\vec{k}) \right] \otimes \left[G^{\mathrm{R}}(\vec{q}_1) \sigma^x G^{\mathrm{A}}(\vec{q}_1) G^{\mathrm{A}}(-\vec{k}) \right]$$
$$= \frac{\pi}{16} \rho(E_{\mathrm{F}}) \left(\frac{2\tau_{\mathrm{e}}}{\hbar} \right)^3 \left[\mathbb{1} \otimes \mathbb{1} - \sigma^x \otimes \sigma^x \right]. \tag{B.8}$$

Summing these three contributions we obtain

$$H^{\mathrm{C}} = \rho(E_{\mathrm{F}}) \left(\frac{2\tau_{\mathrm{e}}}{\hbar} \right)^3 \frac{\pi}{16} \left[\sigma^x \otimes \sigma^x + \sigma^y \otimes \sigma^y - 2\, \mathbb{1} \otimes \mathbb{1} \right]. \tag{B.9}$$

The resulting WAL correction is obtained via the final contraction with a Cooperon propagator, as shown in figure B.1, and leads to the expression

$$\langle \delta\sigma \rangle = \frac{\hbar \rho(E_{\mathrm{F}}) (-e v_{\mathrm{F}})^2}{2\pi} \left(\frac{2\tau_{\mathrm{e}}}{\hbar} \right)^3 \frac{\pi}{16} \mathrm{tr} \left(\sigma^x \otimes \sigma^x + \sigma^y \otimes \sigma^y - 2\, \mathbb{1} \otimes \mathbb{1} \right) \int_{\vec{Q}} \Gamma(\vec{Q})$$
$$= \left(\frac{e^2}{\pi \hbar} \right) \int_{\vec{Q}} \frac{1}{Q^2}. \tag{B.10}$$

Appendix C. Universal conductance fluctuations for Dirac fermions

To derive the conductance fluctuations, we need to take into account two kinds of diagrams containing either Cooperons or Diffusons. The Hikami box for Cooperons has been calculated previously. Proceeding similarly with the Diffuson instead of Cooperon structure factor we obtain the Hikami box for Diffusons:

$$H^{\mathrm{D}} = \rho(E_{\mathrm{F}}) \left(\frac{2\tau_{\mathrm{e}}}{\hbar} \right)^3 \frac{\pi}{16} \left[2\, \mathbb{1} \otimes \mathbb{1} + \sigma^x \otimes \sigma^x + \sigma^y \otimes \sigma^y \right]. \tag{C.1}$$

We have already performed an integration over the momentum (arising from the Kubo formula) in these expressions for the Hikami boxes. Hence we only need to plug a Diffuson (resp. Cooperon) structure factor between two H^{D} (resp. H^{C}). Summing these two diagrams (figures C.1 and C.2), we obtain

$$\langle \delta\sigma_1^2 \rangle = 8 \left(\frac{e^2}{h} \right)^2 \frac{1}{V} \int_{\vec{q}} \frac{1}{q^4}. \tag{C.2}$$

The second part of the conductance fluctuations comes from the diagrams represented in figure C.3 that we have not yet considered. They require the determination of two additional Hikami boxes (one for Diffusons and one for Cooperons):

$$\tilde{H}^{\mathrm{D}} = \rho(E_{\mathrm{F}}) \left(\frac{2\tau_{\mathrm{e}}}{\hbar} \right)^3 \frac{\pi}{16} \left[m1 \otimes \mathbb{1} + \sigma^x \otimes \sigma^x \right], \tag{C.3}$$

$$\tilde{H}^{\mathrm{C}} = \rho(E_{\mathrm{F}}) \left(\frac{2\tau_{\mathrm{e}}}{\hbar} \right)^3 \frac{\pi}{16} \left[\mathbb{1} \otimes \mathbb{1} - \sigma^x \otimes \sigma^x \right]. \tag{C.4}$$

The final results after contraction in spin space of these diagrams is

$$\langle \delta\sigma_2^2 \rangle = 4 \left(\frac{e^2}{h} \right)^2 \frac{1}{V} \int_{\vec{q}} \frac{1}{q^4}. \tag{C.5}$$

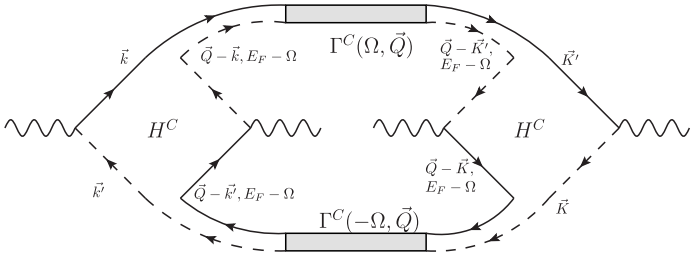

Figure C.1. Diagram for the conductance fluctuations with Cooperons.

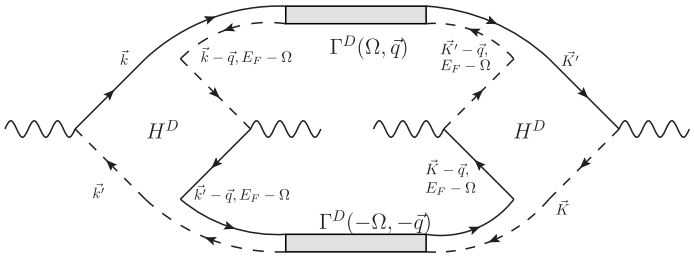

Figure C.2. Diagram for the conductance fluctuations with Diffusons.

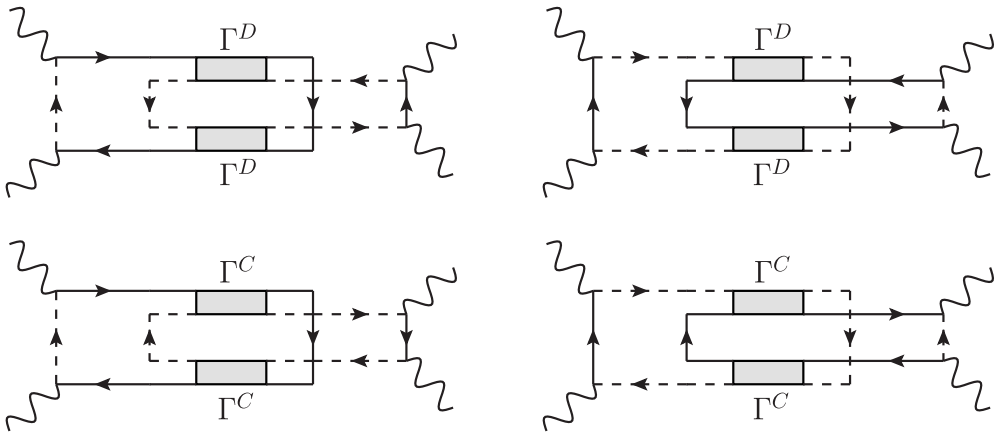

Figure C.3. Diagrams for the second contribution to conductance fluctuations.

Summing the two contributions (C.2) and (C.5), we finally get the result of equation (33):

$$\langle \delta\sigma^2 \rangle = \langle \delta\sigma_1^2 \rangle + \langle \delta\sigma_2^2 \rangle = 12 \left(\frac{e^2}{h}\right)^2 \frac{1}{V} \int_{\vec{q}} \frac{1}{q^4}. \tag{C.6}$$

Appendix D. Quantum correction for a warped Fermi surface

Appendices B and C show explicitly the derivation of the WAL correction and the conductance fluctuations for Dirac fermions. As expected, the corresponding results display no dependence in the only relevant parameter to characterize diffusion: the diffusion constant. These results are naturally expected to hold when taking into account the HW term. To explicitly show this

independence, we determine the value of the quantum correction to conductivity in the general case where the Fermi surface possesses the hexagonal deformation.

The first step is to obtain the new Hikami box H^{C}, the difficulty arising from the dependence of the current operator on the momentum $j_x = e(-v_{\mathrm{F}}\sigma_x + \frac{3\lambda}{\hbar}\sigma_z(k_x^2 - k_y^2))$. Recalling that $\Sigma^x = j_x + j_x P^{\mathrm{D}}\Gamma^{\mathrm{D}}$, we express the 'naked' Hikami box as

$$H_0^{\mathrm{C}} = \int_{\vec{k}} \left[G^{\mathrm{A}}(\vec{k})\Sigma^x G^{\mathrm{R}}(\vec{k}) G^{\mathrm{R}}(-\vec{k})\Sigma^x G^{\mathrm{A}}(-\vec{k}) \right]. \tag{D.1}$$

We perform this integral using polar coordinates, and integrate the radial part:

$$H_0^{\mathrm{C}} = \frac{e^2 v_{\mathrm{F}}^2 \tau_{\mathrm{e}}^2}{4\gamma\hbar} \frac{\tau_{\mathrm{e}}}{\tau_{\mathrm{e}}^{(0)}} \int \frac{\mathrm{d}\theta}{2\pi} \frac{A_+ B A_+ \otimes A_- B A_-}{1 + 12 b^2 \tilde{k}(\theta)^4 \cos^2(3\theta)}, \tag{D.2}$$

$$A_\pm = \mathbb{1} \pm \tilde{k}(\theta)\,(\cos\theta\sigma^x + \sin\theta\sigma^y) + 2b\,\tilde{k}^3(\theta)\cos(3\theta)\sigma^z, \tag{D.3}$$

$$B = \left(2 + \frac{\beta}{\alpha+\beta}\right)\sigma^x + 6b\,\tilde{k}^2(\theta)\cos(2\theta)\sigma^z. \tag{D.4}$$

The two 'dressed' Hikami boxes, where an impurity line links two Green's functions, can be calculated by the method used above, and we can write the result as $H^{\mathrm{C}} = \frac{e^2 v_{\mathrm{F}}^2 \tau_{\mathrm{e}}^2}{4\gamma\hbar} H(b)$. We need to close this Hikami box with a Cooperon structure factor $\Gamma^{\mathrm{C}} = \frac{\gamma}{\tau_{\mathrm{e}}} \frac{1}{D(b)Q^2} \frac{1}{4}\,(\mathbb{1}\otimes\mathbb{1} - \sigma^x\otimes\sigma^x - \sigma^y\otimes\sigma^y - \sigma^z\otimes\sigma^z)$. Performing the sum on the spin space $h(b) = \mathrm{tr}[H(b)\frac{1}{4}\,(\mathbb{1}\otimes\mathbb{1} - \sigma^x\otimes\sigma^x - \sigma^y\otimes\sigma^y - \sigma^z\otimes\sigma^z)]$, we obtain the quantum correction to the conductivity:

$$\langle \delta\sigma(b)\rangle = \frac{\hbar}{2\pi}\mathrm{Tr}(H^{\mathrm{C}}\Gamma^{\mathrm{C}}) = \frac{e^2}{h}\frac{v_{\mathrm{F}}^2\tau_{\mathrm{e}} h(b)}{2D(b)} \int \frac{\mathrm{d}\vec{q}}{q^2}. \tag{D.5}$$

We found numerically the correction $\frac{v_{\mathrm{F}}^2\tau_{\mathrm{e}} h(b)}{2D(b)}$ to be constantly equal to 1 and independent of b.

References

[1] Hasan M Z and Kane C L 2010 Colloquium: topological insulators *Rev. Mod. Phys.* **82** 3045

[2] Qi X-L and Zhang S-C 2011 Topological insulators and superconductors *Rev. Mod. Phys.* **83** 1057

[3] Zhang H, Liu C-X, Qi X-L, Dai X, Fang Z and Zhang S-C 2009 Topological insulators in Bi_2Se_3, Bi_2Te_3 and Sb_2Te_3 with a single Dirac cone on the surface *Nature Phys.* **5** 438

[4] Xia Y *et al* 2009 Observation of a large-gap topological-insulator class with a single Dirac cone on the surface *Nature Phys.* **5** 398

[5] Chen Y L *et al* 2009 Experimental realization of a three-dimensional topological insulator, Bi_2Te_3 *Science* **325** 178–81

[6] Hsieh D *et al* 2009 A tunable topological insulator in the spin helical Dirac transport regime *Nature* **460** 1101

[7] Eto K, Ren Z, Taskin A, Segawa K and Ando Y 2010 Angular-dependent oscillations of the magnetoresistance in Bi_2Se_3 due to the three-dimensional bulk Fermi surface *Phys. Rev.* B **81** 195309

[8] Analytis J, Chu J, Chen Y, Corredor F, McDonald R, Shen Z and Fisher I 2010 Bulk Fermi surface coexistence with Dirac surface state in Bi_2Se_3: a comparison of photoemission and Shubnikov–de Haas measurements *Phys. Rev.* B **81** 205407

[9] Butch N, Kirshenbaum K, Syers P, Sushkov A, Jenkins G, Drew H and Paglione J 2010 Strong surface scattering in ultrahigh-mobility Bi_2Se_3 topological insulator crystals *Phys. Rev.* B **81** 241301

[10] Analytis J G, McDonald R D, Riggs S C, Chu J-H, Boebinger G S and Fisher I R 2010 Two-dimensional surface state in the quantum limit of a topological insulator *Nature Phys.* **6** 960
[11] Checkelsky J G, Hor Y S, Cava R J and Ong N P 2011 Bulk band gap and surface state conduction observed in voltage-tuned crystals of the topological insulator Bi_2Se_3 *Phys. Rev. Lett.* **106** 196801
[12] Steinberg H, Gardner D, Lee Y and Jarillo-Herrero P 2010 Surface state transport and ambipolar electric field effect in Bi_2Se_3 nanodevices *Nano Lett.* **10** 5032
[13] Kim D, Cho S, Butch N P, Syers P, Kirshenbaum K, Paglione J and Fuhrer M S 2011 Minimum conductivity and charge inhomogeneity in Bi_2Se_3 in the topological regime arXiv:1105.1410
[14] Kong D, Dang W, Cha J J, Li H, Meister S, Peng H, Liu Z and Cui Y 2010 Few-layer nanoplates of Bi_2Se_3 and Bi_2Te_3 with highly tunable chemical potential *Nano Lett.* **10** 2245
[15] Bouvier C, Meunier T, Ballet P, Baudry X, Kramer R and Levy L 2011 Strained HgTe: a textbook 3D topological insulator arXiv:1112.2092
[16] He H-T, Wang G, Zhang T, Sou I-K, George Wong K L, Wang J-N, Lu H-Z, Shen S-Q and Zhang F-C 2011 Impurity effect on weak antilocalization in the topological insulator Bi_2Te_3 *Phys. Rev. Lett.* **106** 166805
[17] Culcer D, Hwang E H, Stanescu T D and Das Sarma S 2010 Two-dimensional surface charge transport in topological insulators *Phys. Rev.* B **82** 155457
[18] Fu L 2009 Hexagonal warping effects in the surface states of the topological insulator Bi_2Te_3 *Phys. Rev. Lett.* **103** 266801
[19] Alpichshev Z, Analytis J G, Chu J-H, Fisher I R, Chen Y L, Shen Z X, Fang A and Kapitulnik A 2010 STM imaging of electronic waves on the surface of Bi_2Te_3: topologically protected surface states and hexagonal warping effects *Phys. Rev. Lett.* **104** 016401
[20] Alpichshev Z, Analytis J G, Chu J-H, Fisher I R and Kapitulnik A 2011 STM imaging of a bound state along a step on the surface of the topological insulator Bi_2Te_3 *Phys. Rev.* B **84** 041104
[21] Souma S, Kosaka K, Sato T, Komatsu M, Takayama A, Takahashi T, Kriener M, Segawa K and Ando Y 2011 Direct measurement of the out-of-plane spin texture in the Dirac-cone surface state of a topological insulator *Phys. Rev. Lett.* **106** 216803
[22] Xu S-Y *et al* 2011 Realization of an isolated Dirac node and strongly modulated spin texture in the topological insulator Bi_2Te_3 arXiv:1101.3985
[23] Jung W *et al* 2011 Observation of warping effects in the band and angular momentum structures of topological insulator Bi_2Te_3 arXiv:1112.2476
[24] Kuroda K *et al* 2010 Hexagonally deformed Fermi surface of the 3D topological insulator Bi_2Se_3 *Phys. Rev. Lett.* **105** 076802
[25] Hirahara T, Sakamoto Y, Takeichi Y, Miyazaki H, Kimura S-I, Matsuda I, Kakizaki A and Hasegawa S 2010 Anomalous transport in an *n*-type topological insulator ultrathin Bi_2Se_3 film *Phys. Rev.* B **82** 155309
[26] Yazyev O V, Moore J E and Louie S G 2010 Spin polarization and transport of surface states in the topological insulators Bi_2Se_3 and Bi_2Te_3 from first principles *Phys. Rev. Lett.* **105** 266806
[27] Tkachov G and Hankiewicz E M 2011 Weak antilocalization in HgTe quantum wells and topological surface states: massive versus massless Dirac fermions *Phys. Rev.* B **84** 035444
[28] Wang C M and Yu F J 2011 Effects of hexagonal warping on surface transport in topological insulators *Phys. Rev.* B **84** 155440
[29] Schnyder A P, Ryu S, Furusaki A and Ludwig A W W 2008 Classification of topological insulators and superconductors in three spatial dimensions *Phys. Rev.* B **78** 195125
[30] Schnyder A P, Ryu S, Furusaki A and Ludwig A W W 2009 Classification of topological insulators and superconductors *AIP Conf. Proc.* **1134** 10–21
[31] Bardarson J H, Tworzydło J, Brouwer P W and Beenakker C W J 2007 One-parameter scaling at the Dirac point in graphene *Phys. Rev. Lett.* **99** 106801
[32] Nomura K, Koshino M and Ryu S 2007 Topological delocalization of two-dimensional massless Dirac fermions *Phys. Rev. Lett.* **99** 146806

[33] Ostrovsky P M, Gornyi I V and Mirlin A D 2010 Interaction-induced criticality in z_2 topological insulators *Phys. Rev. Lett.* **105** 036803
[34] Liu C-X, Qi X-L, Zhang H J, Dai X, Fang Z and Zhang S-C 2010 Model Hamiltonian for topological insulators *Phys. Rev.* B **82** 045122
[35] McCann E, Kechedzhi K, Fal'ko V I, Suzuura H, Ando T and Altshuler B L 2006 Weak-localization magnetoresistance and valley symmetry in graphene *Phys. Rev. Lett.* **97** 146805
[36] Akkermans E and Montambaux G 2007 *Mesoscopic Physics of Electrons and Photons* (Cambridge: Cambridge University Press)
[37] Altland A and Zirnbauer M R 1997 Nonstandard symmetry classes in mesoscopic normal–superconducting hybrid structures *Phys. Rev.* B **55** 1142
[38] Evers F and Mirlin A D 2008 Anderson transitions *Rev. Mod. Phys.* **80** 1355
[39] Tikhonenko F V, Kozikov A A, Savchenko A K and Gorbachev R V 2009 Transition between electron localization and antilocalization in graphene *Phys. Rev. Lett.* **103** 226801
[40] Kharitonov M and Efetov K B Yu 2008 Universal conductance fluctuations in graphene *Phys. Rev.* B **78** 033404
[41] Glasser M L 1973 The evaluation of lattice sums. I. Analytic procedures *J. Math. Phys.* **14** 409
[42] Abramowitz M and Stegun I 1972 *Handbook of Mathematical Functions* (New York: Dover)